Supplementary Information (SI) for Journal of Materials Chemistry C.
This journal is © The Royal Society of Chemistry 2024

Supplementary Information

Deciphering the carrier dynamics enhancement in WO_3-containing composites: an ultrafast transient reflectance investigation

Haijuan Zhang, *[ab] Tianxiang Jiang, [c] Meiqiong Zhan, [a] Haiping Li *[d] and Faming Lu *[b]

[a.] *School of Mathematics, Physics and Statistics, Shanghai Polytechnic University, Shanghai 201209, China.*

[b.] *Center for Ultrafast Science and Technology and School of Physics and Astronomy, Shanghai Jiao Tong University, Shanghai 200240, China.*

[c.] *School of Energy and Materials, Shanghai Polytechnic University, Shanghai 201209, China*

[d.] *National Engineering Research Center for Colloidal Materials, School of Chemistry and Chemical Engineering, Shandong University, Jinan 250100, China.*

**All correspondence should be addressed: F. Lu (faminglu@sjtu.edu.cn); H. Li (hpli@sdu.edu.cn); H. Zhang (zhanghj@sspu.edu.cn).*

S1. Preparation for WO_3, $Li_{0.1}WO_3$ and $FeOOH/Li_{0.1}WO_3$

The three samples were synthesized using an in situ solvothermal method following Ref. 3. Typically, for the preparation of WO_3, 0.5 mmol of WCl_6 was dissolved in 40 mL of absolute ethanol and stirred for 40 minutes. Subsequently, 8 mL of CH_3COOH was added, followed by an additional 10 minutes of stirring, resulting in a homogeneous precursor solution. This solution was then transferred into a Teflon-lined stainless steel autoclave, sealed, and heated at 200 °C for 30 hours in an oven. The resulting WO_3 sample was collected, washed with deionized water several times, and dried at 50 °C in an oven for 6 hours to yield pure WO_3. The synthesis of $Li_{0.1}WO_3$ followed a similar procedure to that of WO_3, with one additional step: 17 mg of $LiNO_3$ was introduced along with CH_3COOH during the preparation of the precursor solution.

The fabrication of $FeOOH/Li_{0.1}WO_3$ commenced with the dissolution of 1 mmol of $FeCl_3{\cdot}6H_2O$ in 40 mL of absolute ethanol, stirred for 5 minutes. Then, 200 mg of pre-synthesized $Li_{0.1}WO_3$ was added to the solution and subjected to ultrasonication for 10 minutes. Following this, 3 mmol of NH_4HCO_3 was incorporated into the mixture and stirred for 8 hours, leading to the formation of amorphous FeOOH on the surface of $Li_{0.1}WO_3$. Ultimately, the product was collected by centrifugation, washed with deionized water several times, and dried under vacuum at 50 °C for 6 hours to obtain the $FeOOH/Li_{0.1}WO_3$ composite.

S2. Survey XPS spectra of WO_3, $Li_{0.1}WO_3$ and $FeOOH/Li_{0.1}WO_3$

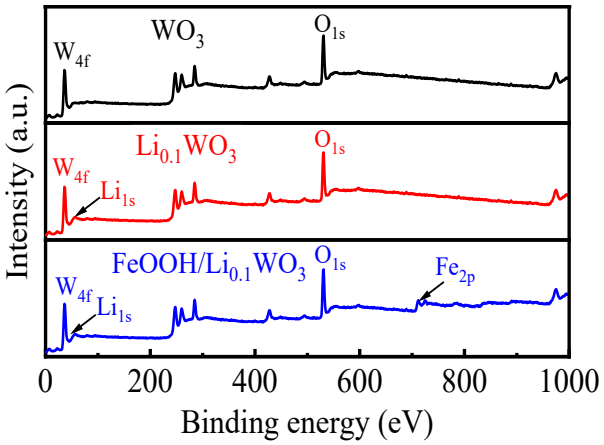

Fig. S1 Survey XPS spectra of WO_3, $Li_{0.1}WO_3$ and FeOOH/$Li_{0.1}WO_3$.

S3. Transient reflectance measurements

Transient Reflectance (TR) measurements were conducted using a 1 kHz Ti:sapphire laser system (Legend Elite HE+USP-III, Coherent, Inc.), which provides 40 fs pulses at a central wavelength of 800 nm. In the case of 800 nm pump-800 nm probe measurements, the laser output was divided into two beams by a 9:1 beam splitter, with the more intense beam designated as the pump and the less intense one as the probe. For the 400 nm pump-800 nm probe measurements, the 400 nm pump beam was generated through second harmonic generation using Type I BBO crystals.

For both measurement setups, the pump spot diameter was approximately 2 mm, significantly larger than that of the probe spot at 0.2 mm, facilitating spatial overlap of the two beams. The pump fluence was adjusted from 100 to 580 μJ/cm², while the probe fluence was maintained at approximately 10 μJ/cm². The TR signal was acquired by altering the temporal interval between the pump and probe pulses, utilizing a high-precision delay stage positioned in the pump beam's path. Throughout data acquisition, the pump beam was modulated at 220 Hz by an optical chopper, and the resultant intensity changes of the reflected probe beam were collected using the lock-in amplification technique.

S4. Interpretation of the carrier dynamics detected by 800 nm probe under 400 nm and 800 nm pump in TR measurements.

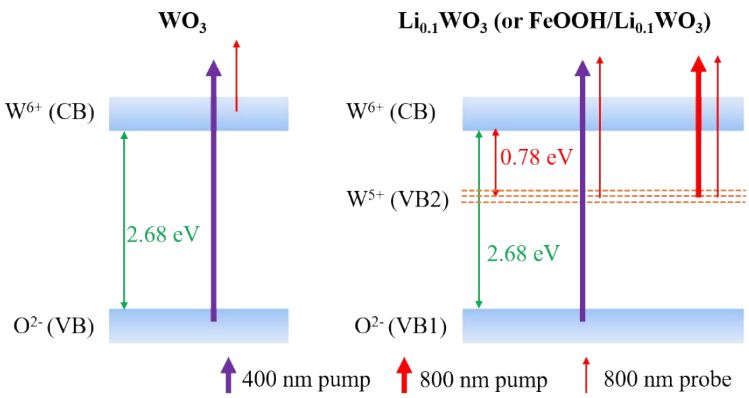

Scheme S1. Schematic diagram of the carrier dynamics detected by 800 nm probe under 400 nm and 800 nm pump in TR measurements.

As detailed in the main text, WO_3 possesses an intrinsic bandgap of approximately 2.68 eV, with the *2p* orbitals of O^{2-} constituting the valence band (VB) and the *5d* orbitals of W^{6+} forming the conduction band (CB). In contrast, $Li_{0.1}WO_3$ and FeOOH/$Li_{0.1}WO_3$ exhibit an additional bandgap of approximately 0.78 eV due to the formation of a new valence band (VB2 as depicted in Scheme S1) induced by lithium intercalation. Due to the varying band structure distributions of the above materials, the 800 nm wavelength probes the dynamics of carriers on different bands across them, as discussed in the following.

For clarity, we will explore this subject across three distinct scenarios: **Case I** involves WO_3 being pumped at 400 nm and probed at 800 nm; **Case II** pertains to $Li_{0.1}WO_3$ (or FeOOH/$Li_{0.1}WO_3$) being pumped at 400 nm and probed at 800 nm; **Case III** examines $Li_{0.1}WO_3$ (or FeOOH/$Li_{0.1}WO_3$) when both pumped and probed at 800 nm.

In **Case I**, 400 nm photons, with an energy of 3.10 eV that surpasses the 2.68 eV bandgap of WO_3, are anticipated to induce a transition from the O^{2-} *2p* to the W^{6+} *5d* levels (as depicted by thick purple arrows in Scheme S1 on the WO_3 panel). Here, the 800 nm photons are capable of directly monitoring the dynamics of photo-excited electrons in the CB (illustrated by thin red arrows in Scheme S1 on the WO_3 panel), given that their photon energies are insufficient to bridge the 2.68 eV bandgap.

For **Case II**, although the 400 nm photons stimulate an O^{2-} *2p* to W^{6+} *5d* transition in $Li_{0.1}WO_3$ and FeOOH/$Li_{0.1}WO_3$, akin to WO_3 (as indicated by thick purple arrows in Scheme S1 on the respective panels), the 800 nm wavelength primarily investigates the carrier dynamics on the VB2 level (illustrated as thin red arrows in Scheme S1 on the $Li_{0.1}WO_3$ and FeOOH/$Li_{0.1}WO_3$ panel), which lies 0.78 eV (or less than 1.55 eV) below the CB. [24] The rationale is that electrons initially present in VB2, which are greatly outnumbered the photo-excited electrons in the CB, are more responsive to the probing photons. It should be noted that, with a 400 nm pump, both transitions from O^{2-} *2p* to W^{6+} *5d* and from W^{5+} *5d* to W^{6+} *5d* can be excited. However, considering that in the $Li_{0.1}WO_3$ and FeOOH/$Li_{0.1}WO_3$ samples used in this study, lithium is added in very small quantities, the number of electrons on W^{5+} *5d* is significantly lower than those on O^{2-} *2p*. Consequently, the 400 nm photons will be preferentially absorbed by the electrons on O^{2-} *2p*.

This interpretation is supported by the differential reflectance changes observed in Fig. 3 for WO_3 and $Li_{0.1}WO_3$ (or FeOOH/$Li_{0.1}WO_3$). Promptly following the 400 nm excitation, which triggers the same O^{2-} *2p* to W^{6+} *5d* transition across all samples, WO_3's reflectance at 800 nm diminishes, while that of $Li_{0.1}WO_3$ and FeOOH/$Li_{0.1}WO_3$ escalates. This phenomenon can be clarified as follows: after the 400 nm excitation, photo-electrons amass in the CB. For WO_3, which is naturally unresponsive to 800 nm light, this accumulation leads to heightened absorption at 800 nm and a subsequent drop in reflectance. Conversely, in $Li_{0.1}WO_3$ and FeOOH/$Li_{0.1}WO_3$, the electron aggregation in the

CB might reduce the likelihood of VB2 to CB transitions, resulting in diminished absorption and an increase in reflectance at 800 nm.

In **Case III**, 800 nm photons, with their energy of 1.55 eV that is below the 2.68 eV threshold but above the 0.78 eV mark, are expected to catalyze a transition from W^{5+} *5d* to W^{6+} *5d* in $Li_{0.1}WO_3$ and FeOOH/$Li_{0.1}WO_3$ (as shown by the thick red arrow in Scheme S1 on the respective panels). Here, the 800 nm wavelength is also anticipated to scrutinize the carrier dynamics on VB2, in a manner analogous to Case II. This assignment is corroborated by the similar responses of $Li_{0.1}WO_3$ and FeOOH/$Li_{0.1}WO_3$ to the 800 nm probe under both 400 nm and 800 nm excitations. $Li_{0.1}WO_3$ and FeOOH/$Li_{0.1}WO_3$ increases. Same as described for Case II, this increase can be ascribed to the electron accumulation in the CB, which lowers the probability of VB2 to CB transitions, thereby reducing absorption and increasing reflectance at 800 nm.

Above all, it is crucial to recognize that for WO_3, the 800 nm wavelength exclusively monitors the dynamics of photo-electrons in the CB, which is a straightforward process. Whereas for $Li_{0.1}WO_3$ and FeOOH/$Li_{0.1}WO_3$, the dynamics of VB2 electrons fundamentally stem from the behaviors of photo-excited electrons in the CB. Consequently, under either pump condition, the reflectance variation at 800 nm also mirrors the electron dynamics in the CB.

S5. Analysis of carrier dynamics participated by the first and second order mechanisms

As depicted in the inset of Fig. 3a and in Fig. 4c within the main text, the maximum relative transient reflectance change, denoted as $\left(\frac{\Delta R_t}{R}\right)_{max}$, exhibits a linear dependence on the pump fluence, *F*. This relationship takes into account the initial excited carrier density, n_0, which is formulated as $n_0 = F\alpha/hv$, where α represents the sample's absorption coefficient at the pump wavelength, and hv signifies the pump photon energy. Consequently, $\left(\frac{\Delta R_t}{R}\right)_{max}$ can be articulated as a function of n_0: $\left(\frac{\Delta R_t}{R}\right)_{max} = b n_0$. Assuming that the change in transient reflectance, $\Delta R_t/R$, and the transient photo-electron density, n_t, share an identical recovery function, $f(t)$, the equation evolves to $\Delta R_t/R = |\Delta R_t/R|_{max} \cdot f(t) = bn_0 \cdot f(t) = bn_t$. This formulation implies that the observed slow recovery actually corresponds to the depopulation process of photo-electrons within the probed volume.

The depopulation process of photo-carriers in semiconductors is typically characterized by a straightforward rate equation: [25]

$$-\frac{dn_t}{dt} = k_1 n_t + k_2 {n_t}^2 + k_3 {n_t}^3 \quad (1)$$

The terms on the right-hand side are ascribed to: (1) first-order trap state-mediated recombination or carrier diffusion; (2) second-order non-geminate recombination; and (3) third-order Auger

recombination, with k_1, k_2, and k_3 being the respective depopulation rate constants. Given the low pump fluence (100-580 μJ/cm²) utilized in this study, the contribution of the third-order process is considered negligible.

To deepen the comprehension of these dynamics, a preliminary analysis of the experimental data was conducted under the assumption that the recovery process could be predominantly governed by either the first or second-order terms. If the first-order mechanism prevails, Equation (1) simplifies to $-\frac{dn_t}{dt} = k_1 n$, yielding $n_t = n_1 e^{-k_1 t}$. Conversely, if the second-order mechanism is dominant, the equation takes the form $n_t = \frac{n_2}{k_2 n_2 t + 1}$. Here n_1 and n_2 represent the photo-carrier densities depopulated via the first and second-order mechanisms, respectively. Thus, if the first-order mechanism is dominant, the associated change in reflectivity follows the equation $\frac{\Delta R_t}{R} = b n_1 e^{-k_1 t}$, or in logarithmic form, $ln\left(\frac{\Delta R_t}{R}\right) = \ln(b n_1) - k_1 t$, indicating a linear dependence of $ln\left(\frac{\Delta R_t}{R}\right)$ on time delay, t. Similarly, if the second-order mechanism predominates, the reflectivity change aligns with the equation $\frac{\Delta R_t}{R} = b\frac{n_2}{k_2 n_2 t + 1}$ or $\left(\frac{\Delta R_t}{R}\right)^{-1} = \frac{k_2}{b} t + \frac{1}{b n_2}$, signifying a linear relationship of $\left(\frac{\Delta R_t}{R}\right)^{-1}$ with time t.

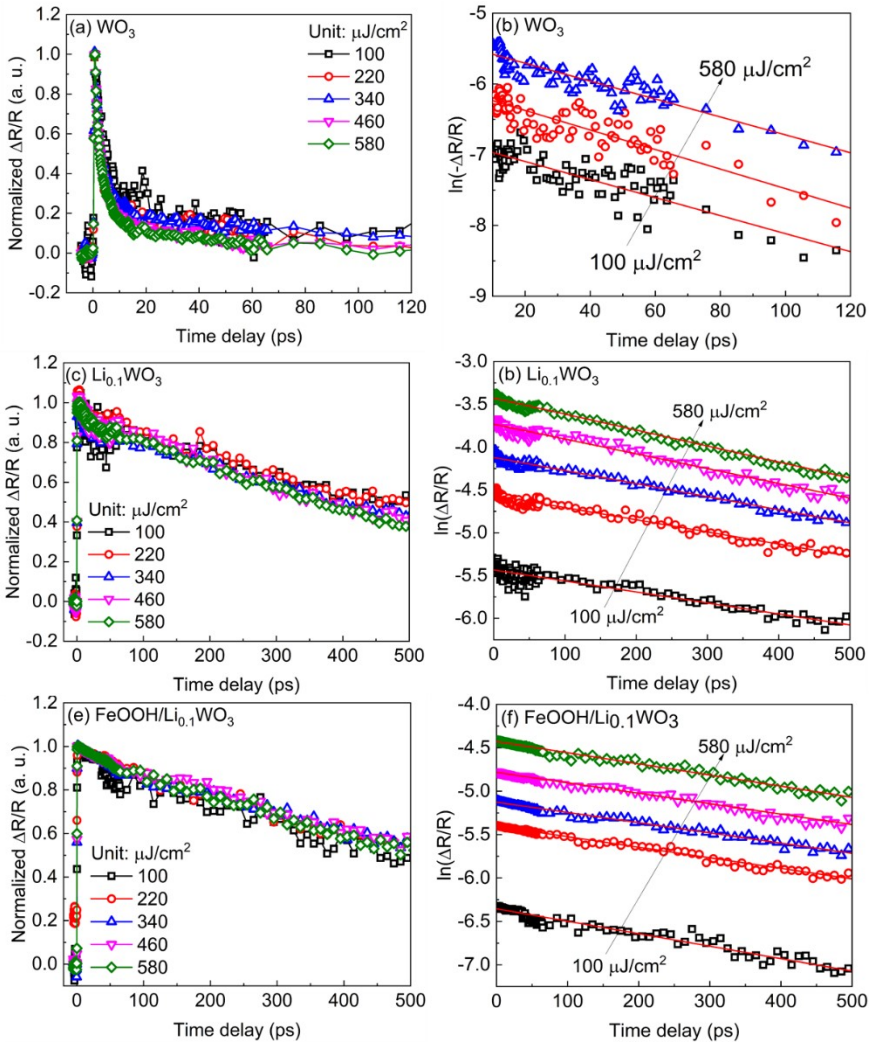

Fig. S2 Relative reflectance change normalized at $(\Delta R/R)_{max}$ for (a) WO_3, (c) $Li_{0.1}WO_3$, and (e) $FeOOH/Li_{0.1}WO_3$ under 400 nm pump and (b), (d), (f) the corresponding time dependences of $\ln(\frac{\Delta R_t}{R})$ during the recovery process. The solid lines in (b), (d) and (f) are linear-fittings to the experimental data presented as scattered points. The arrows indicate the rise in pump fluence.

Figs. S2b, d, and f present the time-dependent $ln\left(\frac{\Delta R_t}{R}\right)$ for WO_3, $Li_{0.1}WO_3$, and $FeOOH/Li_{0.1}WO_3$ under 400 nm excitation, while Figs. S3b and d depict the same for $Li_{0.1}WO_3$ and $FeOOH/Li_{0.1}WO_3$ under 800 nm excitation. The findings indicate that the photo-carrier depopulation in all samples is predominantly governed by a first-order process.

Additionally, it is generally expected that the second-order process would accelerate with increased pump fluence. However, as demonstrated in Fig. S2a, c, e, and S3a, c, the observed depopulation processes are independent of pump fluence, further substantiating the predominance of first-order mechanisms. These outcomes are consistent with the conclusions drawn in the main text, which suggest a minimal involvement of the second-order mechanism.

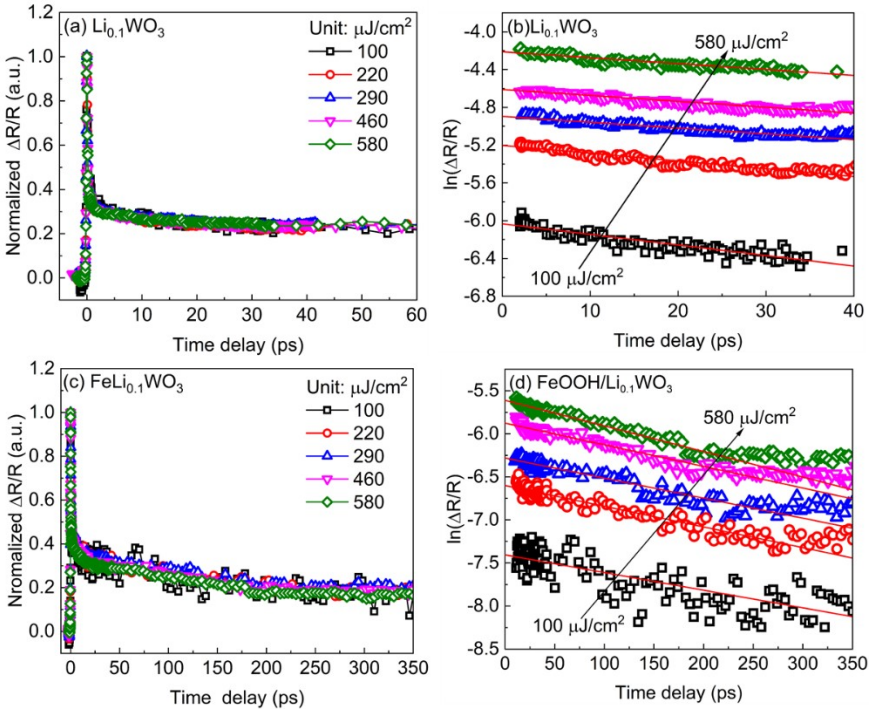

Fig. S3 Relative reflectance change normalized at $(\Delta R/R)_{max}$ for (a) $Li_{0.1}WO_3$ and (c) $FeOOH/Li_{0.1}WO_3$ under 800 nm pump and (b), (d) the corresponding time dependences of $\ln(\frac{\Delta R_t}{R})$ during the recovery process. The solid lines in (b) and (d) are the fitting to the experimental data presented as scattered points. The arrows indicate the rise in pump fluence.